Chemical Engineering Journal 142 (2008) 122–132

Contents lists available at ScienceDirect

Chemical Engineering Journal

journal homepage: www.elsevier.com/locate/cej

Supported nanocomposite catalysts for high-temperature partial oxidation of methane

Tom Sanders[a], Phae Papas[a], Götz Veser[a,b,*]

[a] Chemical Engineering Department, 1249 Benedum Hall, University of Pittsburgh, Pittsburgh, PA 15261, United States
[b] National Energy Technology Laboratory, U.S. Department of Energy, Pittsburgh, PA, United States

ARTICLE INFO

Article history:
Received 11 November 2007
Received in revised form 24 March 2008
Accepted 10 April 2008

Keywords:
Nanocatalysis
Nanocomposite materials
High-temperature catalysis
Catalytic partial oxidation
Synthesis gas
Hydrogen production

ABSTRACT

In order to utilize the vast potential of nanoparticles for industrial catalysis, it is necessary to develop methods to stabilize these particles at realistic technical conditions and to formulate nanoparticle-based catalysts in a way that facilitates handling and reduces health and safety concerns. We have previously demonstrated that metal nanoparticles can be efficiently stabilized by embedding them into a high-temperature stable nanocomposite structure. Building onto these results, we report here on the next step towards a simple, hierarchically structured catalyst via supporting platinum barium-hexaaluminate (Pt-BHA) nanocomposites onto a range of different conventional and novel support structures (monoliths, foams, and felts). The catalysts were characterized via SEM, TEM, XRD, porosimetry, chemisorption, and reactive tests in catalytic partial oxidation of methane to synthesis gas (CPOM), and compared to conventionally prepared Pt-catalysts. In particular silica felt supported Pt-BHA showed excellent activity and selectivity combined with good stability and very low noble metal requirement at the demanding high-temperature conditions of short-contact time CPOM. Overall, we see great potential for these supported nanocomposite catalysts for use in demanding environments, such as high-temperature, high-throughput conditions in fuel processing and similar energy-related applications.

1. Introduction

The exceptional – and sometimes even entirely novel – activity of nanomaterials in combination with recent advances in materials science has lead to an explosive development in "nanocatalysis" over the past decade [1]. However, there is an increasing disconnection between the discovery and development of nanomaterials and their industrial use. This is due to a number of significant concerns and limitations associated with the use of nanomaterials in an industrial environment. Among those, the limited stability of nanomaterials, in particular at elevated temperatures [2], is a major concern, since it restricts the use of nanocatalysts to low and moderate temperature conditions ($T < 500\,^{\circ}C$). Furthermore, the fine powder form in which nanomaterials are typically synthesized create concerns regarding pressure drop, flow maldistribution, and fluid by-pass, as well as health and environmental concerns due to particle handling and possible particle entrainment. However, conventional procedures such as pelletizing, for example, typically result in compacting or even entirely collapsing of the catalyst structure and hence largely undoes desired characteristics such as the large, accessible surface area. Therefore, there is an increasing need to develop materials which combine the desirable characteristics of nanomaterials with the advantages of "conventional", macroscale materials, i.e. which bridge the gap between nanoscale science and "macroscale" application.

A number of recent studies have attempted to overcome the problems associated with nanopowders through the development of hierarchical nanoscale materials. For example, Costacurta et al. examined mesoporous silica deposited on macroporous ceramic foams [3], and Danumah et al. utilized a dual-templating approach to form a hierarchical porous system consisting of cubic mesoporous walls of macro-porous silica, with application as a molecular sieve [4]. Kuang et al. examined a similar macroporous silica with bimodal mesoporous character [5], while Sen et al. achieved mesoporous silica with tunable pores on three different length scales in the macro-, meso-, micro-porous range from an infiltration of a macroporous polystyrene sphere template [6]. However, all of these studies focus on mesoporous silica, and none report on the stability of the resulting materials in demanding environments, such as high-temperature, reactive conditions.

Directly attaching nanoscale catalytic materials onto typical "macro"-scale support structures (monoliths, foams, felts) can be

* Corresponding author at: University of Pittsburgh, 1232 Benedum Hall, Pittsburgh, PA 15261, United States. Tel.: +1 412 624 1042; fax: +1 412 624 1639.
E-mail address: gveser@engr.pitt.edu (G. Veser).

1385-8947/$ – see front matter © 2008 Elsevier B.V. All rights reserved.
doi:10.1016/j.cej.2008.04.018

considered as a simple alternative to the direct formation of a hierarchically structured material. Such support structures are widely used and well-established in industrial catalysis. Monolithic extruded supports are predominantly used in high-throughput environmental applications, such as automotive exhaust treatment and catalytic combustion, due to the low pressure drop per unit length and attrition/crushing resistance of the structure [7]. Among their limitations, however, are poor heat transfer and lack of radial mixing [8]. Ceramic foams, on the other hand, are characterized by their irregular, open pore structure (~75–85% porous), which allows for improved radial mixing, attrition/crushing resistance, as well as low pressure drop [8]. A largely untested support material in catalysis is ceramic felt. The very open nature of the felt results in low pressure drop, while the fibrous structure offers a high surface area for coating active catalyst material. Additionally, the malleable nature of the felt offers a benefit in terms of flexible catalyst design. To our knowledge, the only systematic studies of ceramic felts as catalyst supports are those of Renken and co-workers who examined noble metals supported on silica and aluminoborosilicate glass fibers in a wide range of catalytic oxidation and hydrogenation reactions [9–15].

None of the above investigations have considered the issue of high-temperature reaction conditions, which is of particular concern in fuel processing applications, such as combustion, partial oxidation, and steam reforming of natural gas. However, much work has been devoted to more conventional "macroscale" catalysts for such applications. For example, Arai and Machida developed hexaaluminates, i.e. thermally stabilized aluminas, which show excellent high-temperature stability in combination with decent combustion activity [16]. Building on this work, Zarur and Ying synthesized hexaaluminates in a reverse microemulsion, obtaining catalysts which showed very low ignition temperatures for methane combustion in particular after doping the hexaaluminate with Ce [17]. However, while these materials are highly efficient combustion catalysts, they do not offer the product selectivity necessary for reactions such as partial oxidation of methane to synthesis gas (CPOM). Noble metals, on the other hand, are known to be highly active and selective for CPOM, but suffer from stability problems at high-temperature conditions [18]. Previously, our group was able to successfully overcome the insufficient high-temperature stability of nanoparticles by anchoring noble metal nanoparticles in a hexaaluminate matrix [19,20]. This resulted in the synthesis of exceptionally active and sinter-resistant platinum-barium hexaaluminate (Pt-BHA) powders which combine the high reactivity of nanosized Pt metal particles with the excellent high-temperature stability of stabilized aluminas.

The present study extends these previous efforts towards a hierarchical catalyst structure by investigating the anchoring of nanocomposite Pt-BHA catalyst on different conventional and novel catalyst supports (monoliths, foams, and felts). Catalytic partial oxidation of methane to synthesis gas (CPOM) is chosen as test reaction to evaluate the activity and stability of these structured catalysts due to its industrial importance as well as its high-temperature and short-contact time reaction conditions. In CPOM, methane reacts directly with oxygen or air to form synthesis gas (CO and H_2) in a one-step reaction:

$$CH_4 + 0.5O_2 = CO + 2H_2 \quad (\Delta H_R^0 = -37\,\text{kJ/mol})$$

making it a promising alternative to the traditional industrial route to syngas via steam reforming of methane (SRM) [21]. CPOM is typically catalyzed by noble metals (Pt, Rh), runs auto-thermally due to its mild exothermicity, and is characterized by very high reaction temperatures (>1000 K), extremely short-contact times (<10 ms), and very high reaction rates. These features of the reaction, as well as our previous experience with CPOM [19,22–25] make it an ideal test reaction for the present investigations.

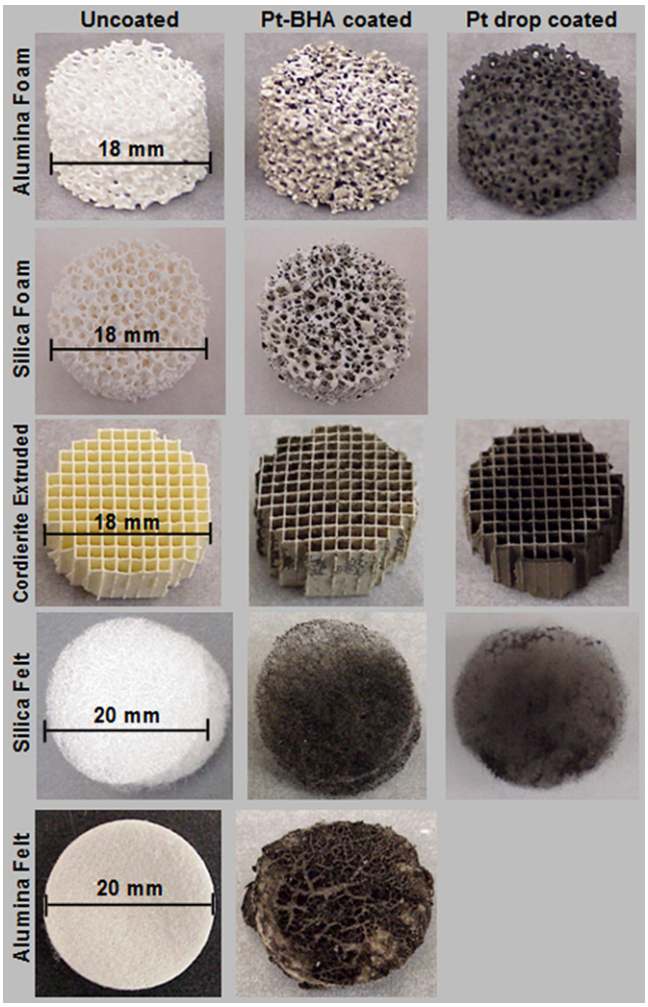

Fig. 1. Images of support structures used for coating and reactive testing. Left-most images are as-received, center are after dip coating with Pt-BHA, right-most after drop coating with Pt-salt solution.

2. Experimental

Pt-BHA was synthesized via a reverse-microemulsion templated pathway described previously [19]. Briefly, a microemulsion was formed from 25.6 g water, 90 g *iso*-octane, 350 g pentanol, and 30 g poly(ethylene glycol)-block-poly(propylene glycol)-block-poly(ethylene glycol) surfactant (M_n = 2000). Chloroplatinic acid hexahydrate (0.86 g) was added to the water phase prior to forming the microemulsion. A mixture of aluminum (13.07 g) and barium (1.36 g) isopropoxides dissolved in dry isopropanol (196 g) was carefully added to the microemulsion under an inert atmosphere. The resulting mixture was aged for 70 h and the opaque gel phase was separated via temperature-induced phase separation. After washing with acetone, the material was dried partially, resulting in a gelatinous form which was used in the experiments. One part of the gel was dried to completion and calcined forming a Pt-BHA powder reference material, while the rest was used for the coating procedures described below. The powder was sieved and only the fraction with d > 500 μm was used in the packed bed because of gas bypass issues.

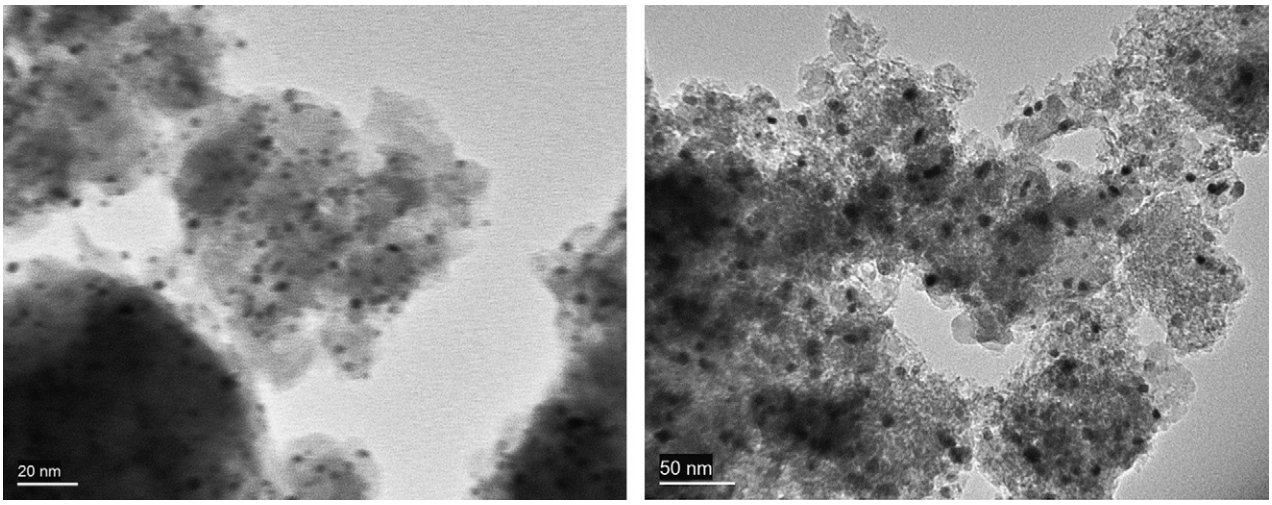

Fig. 2. TEM micrographs of Pt-BHA calcined at 300 °C (left) and 600 °C (right).

Images of the uncoated support structures used are shown in Fig. 1. Alumina and silica foam monoliths were obtained from Vesuvius Hi-Tech Ceramics. Both types of foams are white in color and have 45 pores per linear inch. Cordierite extruded monoliths were obtained from Corning Inc. The monoliths are 400 pores per square inch and initially egg shell colored. Silica felts were obtained from Technical Glass Products. The silica felts had a very open and fibrous nature. Before coating these felts, a chemical binder used in the manufacturing process had to be removed via thermal treatment (1 h at 482 °C in 2 SLM air). Alumina felts were obtained from Zircar ceramics and used as received. The alumina felts had a more densely packed structure than the silica felts.

The dip coating was performed as follows: Each support was placed into a shallow glass vial and covered with a 2–3 ml aliquot of Pt-BHA gel. The gel was allowed to infiltrate the pore network of the support, and the catalysts were dried at ambient conditions overnight. The structures were then calcined in a flow tube oven (3 h at 600 °C in 2 SLM air, followed by 3 h in 10% H_2 in N_2). As a control, separate samples of each support were drop coated with 10 wt% H_2PtCl_6 in distilled water, allowed to dry, and calcined (280 °C, 6 h 1 SLM N_2, 4 h 5% H_2 in N_2). These were chosen as 'conventional' reference materials for the investigations.

Visual inspection of the Pt-BHA coating was done via scanning electron microscopy using a Phillips XL30 electron microscope. Catalyst morphology and platinum particle size are determined by transmission electron microscopy (JEOL-2000FX). Samples for the transmission electron microscopic measurements were obtained by placing a drop of sample suspension in acetone on a copper type-B support grid (Ted Pella, Inc.), followed by air drying to remove the solvent. Pt particle size distributions were determined by counting individual particles in TEM micrographs with the help of ImageJ software [26]. Nitrogen porosimetry (Micromeritics ASAP 2020) was used to determine surface area, pore volume, and pore size distribution. Samples are degassed for 3 h at 200 °C under high vacuum prior to each test. The typical test involved a six-point BET analysis for total surface area measurement and an 84-point Barrett–Joyner–Halenda (BJH) analysis for pore size and volume determination. X-ray diffraction measurements were performed with a high-resolution powder X-ray diffractometer (Phillips PW1830, USA) in line focus mode using a monochromatic Cu radiation at the wavelength of 1.54 Å. Pulse chemisorption of CO (Micromeritics Chemisorb 2750) was used to determine active Pt surface area. Each sample was reduced in a stream of hydrogen gas at 600 °C prior to pulsing with pure CO gas at room temperature.

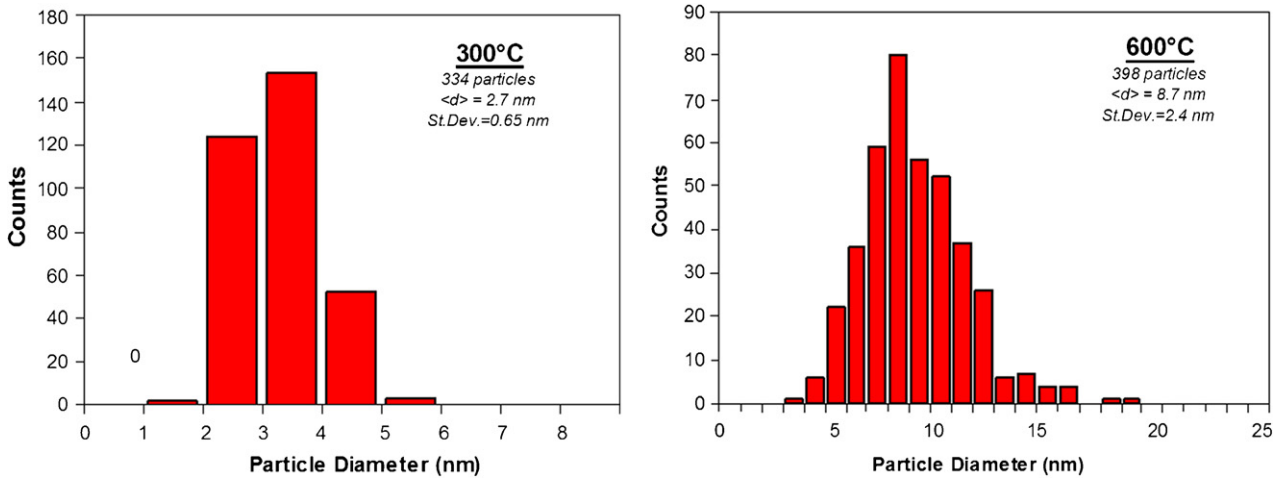

Fig. 3. Pt particle size distributions in Pt-BHA nanocomposite powder catalysts as determined from TEM images.

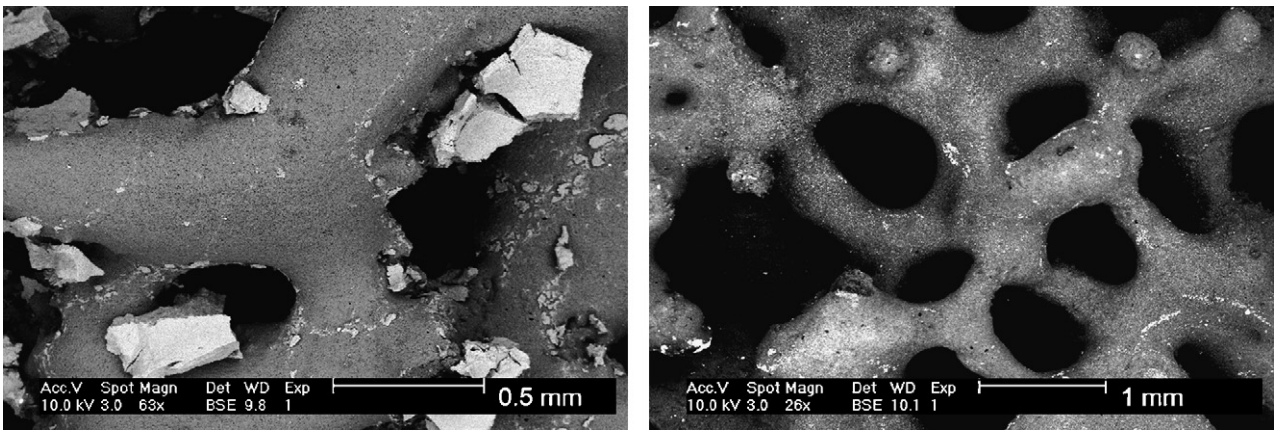

Fig. 4. SEM micrograph of alumina foams. Left: Dip coated with Pt-BHA. Right: Drop coated with Pt-salt solution.

For the reactive tests, all catalysts were wedged between two 10 cm long inert cordierite extruded monoliths, wrapped in a layer of alumina cloth, and inserted into a quartz–glass tube, which was part of a quartz–metal hybrid reactor [19]. K-type thermocouples were used to monitor reaction temperature on either end of the catalyst zone, with typical reaction temperatures between 700 and 1000 °C for all configurations tested. Mass flow controllers (MKS Instruments Inc.) were used to feed the reactants (methane and synthetic air). All tests were run autothermally at 4 SLM total flow rate, resulting in residence times between 9 and 38 ms for the different catalyst configurations (at standard inlet conditions).

3. Results and discussion

Since the aim of the present investigation was the development of a supported nanocomposite catalyst without compromising the underlying activity of the nanoscaled active component, the unsupported, highly active powder form of the nanocomposite Pt-BHA catalyst was used as reference material in the present investigation. The excellent activity, selectivity, and stability of this Pt-BHA nanocomposite powder catalysts had already previously been demonstrated in our group in detailed investigations of catalytic partial oxidation of methane to synthesis gas [19]. In the following, after a brief characterization of this reference material, various supported catalyst formulations – alumina felts, silica foams and felts, and cordierite extruded monoliths – are evaluated with regard to activity, selectivity and stability in comparison to this reference material as well as "conventionally" supported catalysts prepared by drop-coating with Pt-salt solution.

3.1. Characterization of Pt-BHA

First, the unsupported Pt-BHA powder was characterized via TEM. TEM images of Pt-BHA powder after calcination at 300 and 600 °C are shown in Fig. 2. After low-temperature calcination at $T = 300$ °C, the Pt particles (black spots) are small and well dispersed in the barium hexaaluminate matrix (grey substrate). The average particle size is 2.7 nm with a narrow size distribution ($\sigma = 0.65$ nm) as determined from particle size statistics shown in Fig. 3. After calcination at $T = 600$ °C, the particles grow to an average size of 8.7 nm and the size distribution broadens to $\sigma = 2.4$ nm. This particle growth can be correlated with removal of residual surfactant at a calcination temperature of ~450 °C, and the Pt particle size then remains essentially unchanged up to temperatures around 1000 °C [20].

3.2. Coating of different support structures

After supporting this Pt-BHA powder on the different support structures via dip-coating with the gel form of the uncalcined Pt-BHA (see Section 2), the supported catalysts were first characterized qualitatively via SEM.

The alumina foam-supported Pt-BHA catalyst appears to have a low dispersion of the nanocomposite on the support (first row of Fig. 1). Closer inspection confirms a highly non-uniform

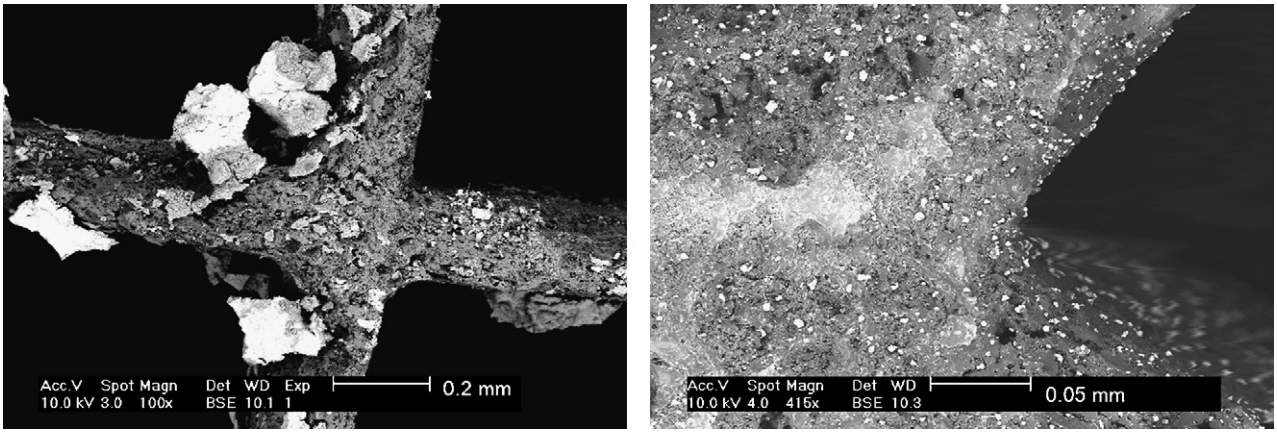

Fig. 5. SEM micrographs of cordierite monoliths. Left: Dip coated with Pt-BHA. Right: Drop coated with Pt-salt solution.

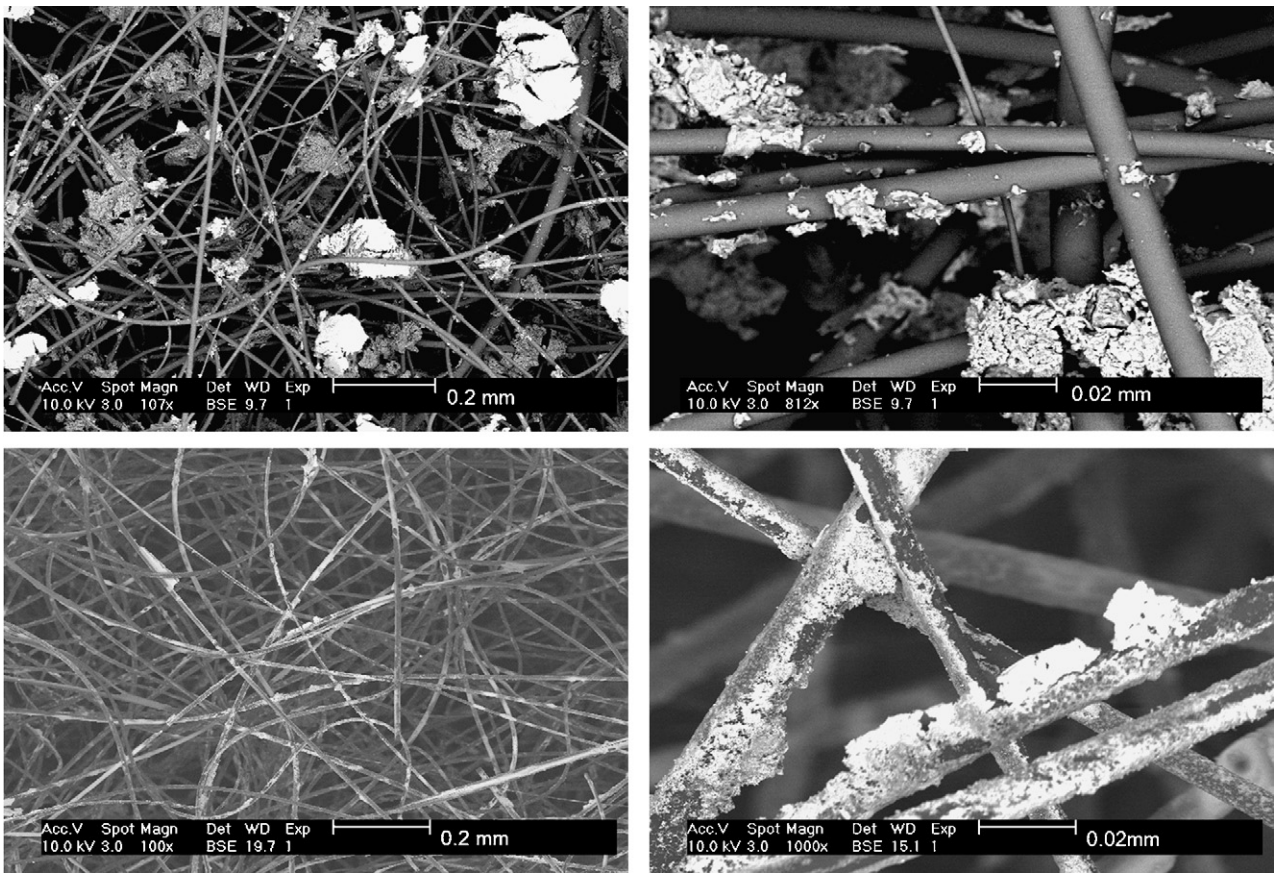

Fig. 6. SEM micrographs of silica felts. Top row: Dip coated with Pt-BHA. Bottom row: Drop coated with Pt-salt solution.

distribution in which large amounts of material are trapped in the inner pore network (Fig. 4, left image). It should be noted that these agglomerates are stable during normal handling and even if the catalyst is mildly tapped onto a surface to shake loose any excess material. Vigorous tapping or other abrasion leads to further loss of catalytic material. In comparison, the alumina foam is also shown after conventional drop-coating with a Pt-salt solution (first row of Fig. 1). This coating leads to a metal coating with a comparatively uniform distribution of Pt on the support structure as confirmed by SEM (Fig. 4, right image).

The silica foam supported Pt-BHA, like the alumina foam supported Pt-BHA, shows a low dispersion of the nanocomposite (second row of Fig. 1), with similar mechanical stability during handling. SEM images of this structure were essentially indistinguishable from those of the alumina foam supported structure, and are therefore not shown. The silica foam was also drop coated with a Pt-salt solution. Again, the properties of this coating were indistinguishable from those of the alumina foam.

The straight-channel cordierite extruded monolith turns grey with small black flecks of Pt-BHA upon coating (third row of Fig. 1). The Pt-BHA material did not have strong adhesion to the cordierite, however, loosing significant amounts of coating even during normal handling of the supported catalyst structure. The nanocomposite is very poorly dispersed on the walls of the monolith structure, as evident in the SEM images shown in Fig. 5 (left image). Adhesion appears to occur predominantly at points in the cordierite structure where the Pt-BHA particles can settle into a fracture or crack. In comparison, the cordierite monolith is also shown again after conventional drop-coating with a Pt-salt solution (third row of Fig. 1). Again this leads to a uniform metal coating with a fairly homogeneous distribution of Pt on the support structure as confirmed by SEM (Fig. 5, right image).

Silica felts were also coated with the Pt-BHA nanocomposite (fourth row of Fig. 1). Visual inspection indicates that the Pt-BHA appears to be well dispersed in the silica fiber structure. The catalyst is stable upon normal handling and mild tapping. Vigorous tapping of the catalyst initially removes a small amount of excess catalytic material, but the majority remains strongly bound to the fibers. SEM images of this silica felt supported Pt-BHA catalyst (Fig. 6, top left micrograph) reveal a “chunky” texture of the material, similar to the Pt-BHA coated foam monoliths. However, a larger number of smaller chunks are adhering to the silica fibers, leading to a better overall dispersion of Pt-BHA. In fact, a closer look reveals additionally a fairly high dispersion of smaller Pt-BHA particles on the fibers (Fig. 6, top right micrograph). Overall, this Pt-BHA dispersion appears to be significantly higher on the silica felts than on any of the other support structures.

In comparison, drop coating the silica felts with 10% H_2PtCl_6 solution leads to a blotchy Pt coating that does not appear very uniform to the naked eye (fourth row of Fig. 1). Beyond this macroscopic inhomogeneity of the coating, however, SEM reveals that each fiber is coated fairly uniformly with a thin layer of Pt (Fig. 6, bottom row).

Finally, Pt-BHA was coated on an alumina felt (final row of Fig. 1). The nanocomposite resides largely on top of the felt and does not penetrate significantly into the fibrous structure. This poor coating is likely due to the fact that the alumina felt is significantly denser than the silica felt, resulting in poor penetration of the coating solution into the fibrous structure. Correspondingly, the mechanical stability of the nanocomposite coating on this structure is very lim-

Table 1
Comparison of active platinum surface area for the supported catalyst structures and the unsupported Pt-BHA powder

Active component	Structure	Size D, L [mm]	m_{Pt} [mg]	A_{Pt} [m^2]	a_{Pt} [m^2/g]	
					[g Pt]	[g cat]
Pt	Alumina foam	18, 10	63	0.29	4.68	0.14
	Silica felt	20, 2	20	0.019	0.96	0.42
Pt-BHA	Alumina foam	18, 10	1.9	0.056	29.6	0.03
	Silica foam	18, 10	2.8	0.11	37.6	0.06
	Silica felt	20, 2	4.8	0.095	19.8	1.15
Pt-BHA	Powder	18, 3	38	2.2	57.4	4.31

ited even during mild handling. Because of this poor stability, this support was not further analyzed and was also not included in the reactive testing.

Overall, these observations seem to indicate that the physical structure of the support is more important for the adhesion of the nanocomposite than the chemical nature, since alumina- and silica-based supports behave very similar in the coating tests, while strong differences existed between the different support structure types.

3.3. Platinum surface area

One of the most important characteristics of a supported catalyst is obviously the amount of exposed active surface area, in this case the total Pt surface area. Therefore, the Pt surface areas of all above described supported nanocomposite catalysts were determined via chemisorption. The results are shown in Table 1. Since all materials are disk shaped, their size is characterized by their respective diameter (D) and length (L). Pt weight loading (m_{Pt}) was calculated based on the ~7.5 wt% Pt in the Pt-BHA nanocomposite used in the coating process. The total platinum surface area (A_{Pt}) was determined using CO pulse chemisorption, and specific surface areas (a_{Pt}) were calculated per mass of platinum and per mass of the entire catalyst (last two columns).

One can see that the total amount of Pt is significantly higher for the catalysts that were drop-coated with a Pt-salt than for those coated with the nanocomposite. This is not surprising since the nanocomposite contains more than 90 wt% BHA and will hence result – for otherwise similar coatings – in a drastically reduced Pt weight loading. However, while one could expect a corresponding decrease in the total Pt surface area for the Pt-BHA coated catalysts, this is only true for the alumina foam catalyst. The silica felt supported Pt-BHA catalyst shows a significantly higher surface area than the conventionally coated felt, indicating a much higher dispersion, i.e. retention of the nanoparticulate nature of the Pt in the nanocomposite coating. This is also reflected in the Pt surface area per total catalyst weight (last column in Table 1), which is higher for the Pt-BHA coated silica felt than for the one coated with pure Pt.

The superior dispersion becomes most apparent in a comparison of the specific Pt surface areas where even the nanocomposite-coated alumina foam shows a six-fold higher specific surface area than the conventionally coated one, while the specific Pt surface area for the silica felt is increased by as much as a factor of 20. In both cases, however, the supporting process leads to the occlusion of some of the Pt, as apparent in a comparison of their specific Pt surface areas with that of the Pt-BHA powder (last row in Table 1). This is of course unavoidable in a supported catalyst, since the active phase has to adhere to the support, making the surface area at the interface between active phase and support inaccessible for the reaction. The fact that the (less stable) alumina foam catalyst shows a lower reduction in specific surface area, i.e. less occlusion than the (more stable) silica felt, indicates that a certain amount of occlusion is even a requirement for a stable adhesion of the nanocomposite to the support.

3.4. Reactive testing

Each of the above discussed supported Pt-BHA catalysts was tested in the catalytic partial oxidation of methane (CPOM) in order to evaluate their activity as well as stability at high-temperature reactive conditions. Experimental results are as shown in Fig. 7,

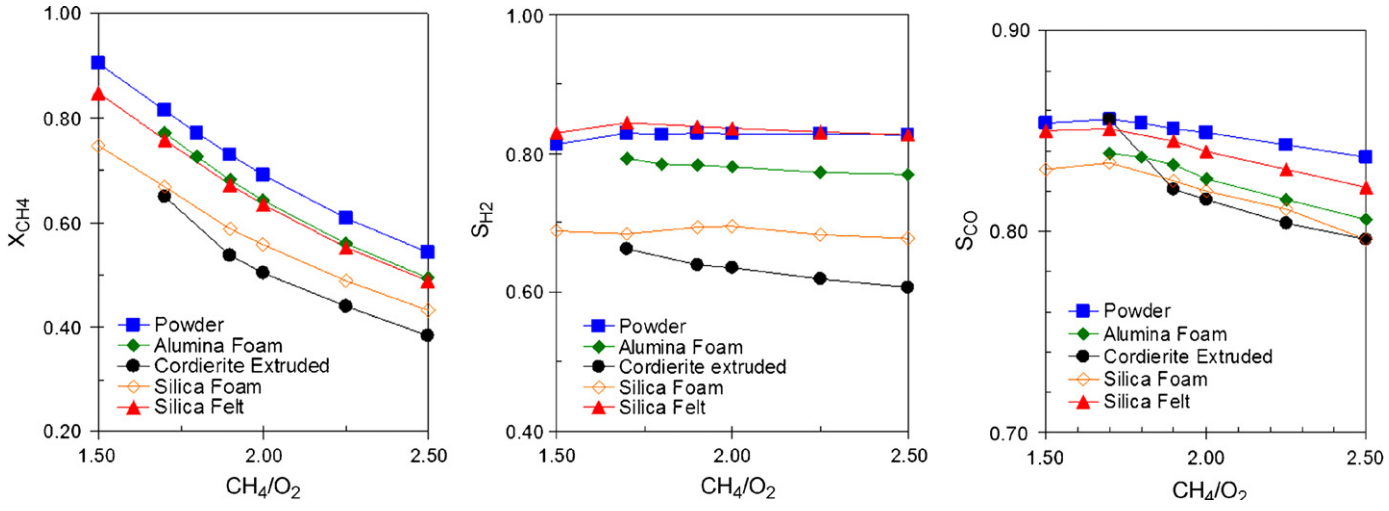

Fig. 7. Methane conversion (left), hydrogen selectivity (center), and carbon monoxide selectivity (right) vs. molar CH_4:O_2 ratio for the supported nanocomposite catalysts in CPOM. Total flow rate = 4.0 SLM, N_2:O_2 = 4:1, autothermal operation.

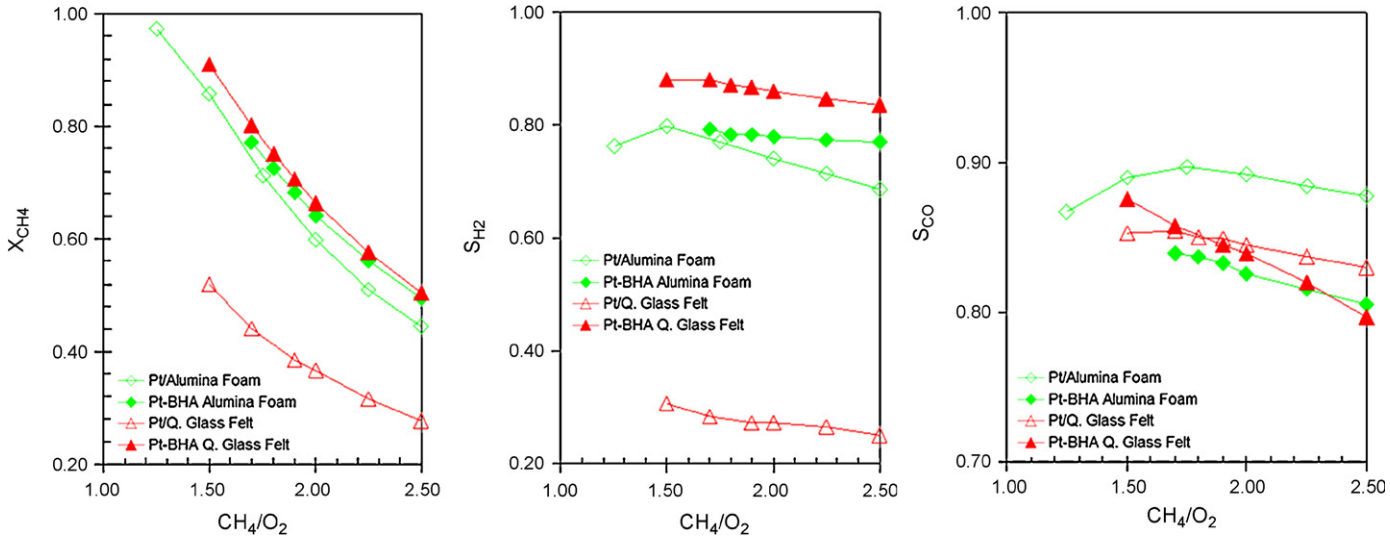

Fig. 8. Methane conversion (left), hydrogen selectivity (center), and carbon monoxide selectivity (right) vs. molar CH_4:O_2 ratio for alumina foam and silica felts coated by drop coating with aqueous platinum solution and dip coating with Pt-BHA gel. Total flow rate = 4.0 SLM, N_2:O_2 = 4:1, autothermal operation.

where methane conversion (left graph), hydrogen selectivity (center) and CO selectivity (right graph) are shown as a function of molar methane-to-oxygen ratio (O_2:N_2 = 1:4) for adiabatic operation at a total flow rate of 4 SLM (standard liters per minute). Oxygen conversion is always complete at the experimental conditions and is hence not shown.

Methane conversion (left graph) decreases monotonically with increasing CH_4/O_2 ratio for all catalysts. This is a well-known trend in CPOM [19,27], and is explained by the fact that oxygen is the limiting reactant in this reaction system, and hence increasing oxygen availability with decreasing CH_4/O_2 ratio results in higher methane conversion. Methane conversion for the powder, foam monolith, and silica felt are identical within experimental error (±3%). The extruded monolith and silica foam monolith perform poorly compared with the other nanocomposite catalysts, with methane conversions as much as 20 and 15% less (respectively) than Pt-BHA powder.

Hydrogen selectivity (center graph) remains almost constant at ~80% (±3%) for the powder, alumina foam, and silica felt for all CH_4/O_2 ratios tested. Again the cordierite extruded monolith and silica foam monolith show significantly lower selectivity than the other supports. This is in agreement with the lower conversions over this catalyst, since a less selective reaction, i.e. a higher degree of total oxidation, consumes more of the limiting reactant (oxygen) due to the stoichiometry of the total oxidation reaction and hence results in lower methane conversion.

Finally, CO selectivity (right hand graph) shows similar values of ~80–85% with a slight decreasing trend with CH_4/O_2 ratio for all catalysts across the whole range of CH_4/O_2 ratios.

These conversions and selectivities are well in excess of those reported previously for conventionally prepared supported Pt catalysts [19,20,27–32]. Strong improvements in methane conversion (by up to 20%) and even more pronounced improvements in hydrogen selectivity (by up to 40% from the conventional catalysts to the nanocomposite powder) are observed across the whole range of methane-to-oxygen ratios. The results over the Pt-BHA nanocomposite powder furthermore are in good agreement with our previous results over a similar type of catalyst [19], attesting to not only the excellent catalytic activity and selectivity of these nanocomposite catalysts, but also to the well-controlled and highly reproducible synthesis procedure.

Temperatures measured at the back-edge of the various catalysts (not shown here) ranged between 730 and 830 °C for Pt-BHA powder, 750 and 830 °C for alumina foam-supported Pt-BHA, 790 and 900 °C for the silica foam, 920 and 1010 °C for the cordierite extruded monolith, and 700 and 810 °C for the silica felt. The temperatures increased monotonically as the methane-to-oxygen ratio decreased from 2.5 to 1.5 due to the increasing methane conversion for leaner mixtures. The average temperature is furthermore strongly affected by changing hydrogen selectivities between the different catalysts and as a function of methane-to-oxygen ratio. This is expected since lower selectivity for hydrogen indicates a higher degree of methane combustion, which is a strongly exothermic process.

Overall, the results indicate that Pt-BHA supported on extruded cordierite monoliths and silica foam monoliths are relatively poor CPOM catalysts. In addition, rapid deactivation was observed over the extruded cordierite monolith to the point where a second ignition of the CPOM reaction after prolonged operation was not possible any more. The low reactivity and poor stability of the extruded monolith appear to reflect the difficulty involved in coating the structure, which leads to low Pt-BHA loadings, poor dispersion of nanocomposite, and diminished catalytic stability. The reasons for the poor performance of the silica foam catalyst are not entirely clear from the present results, as the catalyst showed similar coating, stability, and surface areas as the alumina foam catalyst, yet significantly lower activity and selectivity in the reaction.

In contrast to that, the alumina foam and silica felt supported catalysts offer similar reactivity to the unsupported Pt-BHA powder at a total Pt weight loading that is around an order of magnitude lower. While one could conclude that one could use 10 times less powder, this is not possible as the catalyst bed was already only 3 mm long and a further reduction (even by much less than a factor of 10) would lead to significant problems with maldistribution of the shallow bed and strong gas bypass and channeling. This points to one of the main advantages of using supported nanocomposite powders: using a support structure allows the use of very small amounts of catalyst while maintaining a well-defined flow pattern and uniform distribution of the catalyst in the reactor. Given the highly reactive nature of nanoparticles, this is a significant consideration well beyond the system studied in the present investigation.

In order to obtain a direct comparison between a conventional supported Pt catalyst and the nanocomposite-based catalysts, the

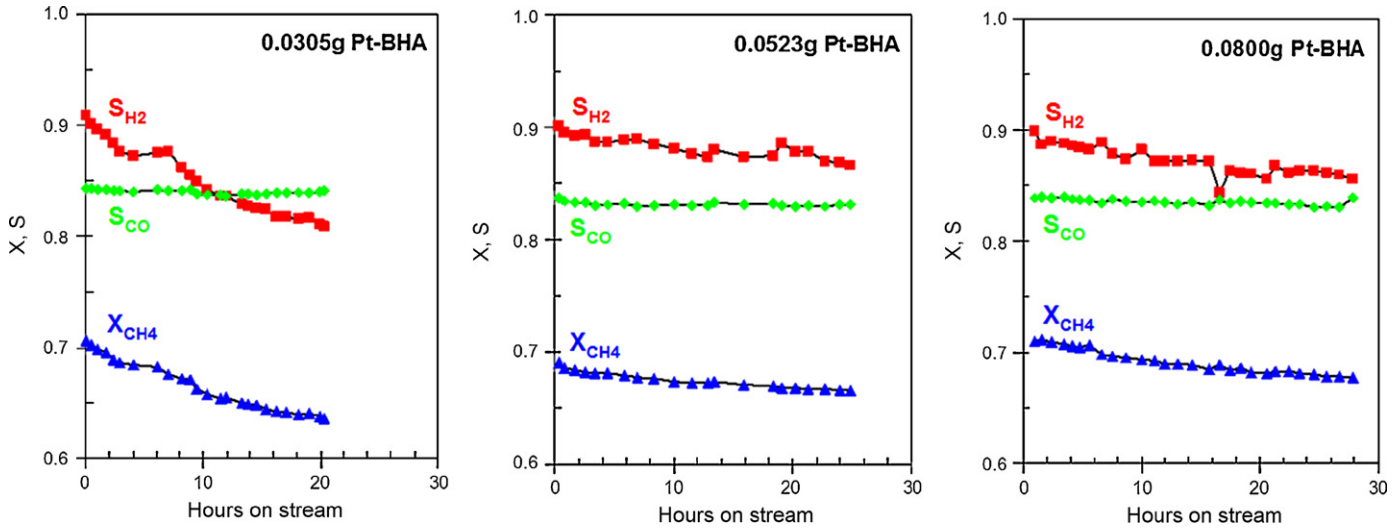

Fig. 9. Methane conversion (triangles), hydrogen selectivity (squares), and carbon monoxide selectivity (diamonds) for silica felts with different weight loading of Pt-BHA nanocomposite in extended operation stability testing. Left: Low weight loading (0.0305 g Pt-BHA), center: medium weight loading (0.0523 g Pt-BHA), right: high weight loading (0.0800 g Pt-BHA). CH_4:O_2 = 2.0, N_2:O_2 = 4:1, total flow rate = 4.0 SLM, autothermal operation.

two most reactive catalysts, the silica felts and alumina foam monoliths, were also evaluated with regard to activity and selectivity in CPOM after drop-coating with H_2PtCl_6. The results are shown in Fig. 8, where methane conversion and H_2 and CO selectivity are shown as a function of CH_4/O_2 ratio in comparison to the results over the equivalent Pt-BHA supported catalysts. One can see that while in both cases the nanocomposite catalysts (closed symbols) outperform the conventional catalysts (open symbols), this improvement is small (albeit significant) for the alumina foam monolith but very pronounced for the silica felt. The reaction temperature also increased for the drop-coated alumina foam (850–990 °C) and silica felt (1010–1150 °C), compared to their Pt-BHA coated counterparts, further indicating the poor syngas selectivity of these catalysts. Again, it should be noted that the nanocomposite catalyst contains more than an order of magnitude less Pt than the drop-coated catalyst (Table 1). The results hence demonstrate that the supported nanocatalysts offers strongly improved activity and selectivity with much lower noble metal requirement than their drop-coated counterparts. In particular the silica felt supported nanocomposite catalyst showed a highly attractive combination of excellent activity and selectivity with good mechanical stability and very easy and flexible handling.

3.5. Catalyst stability

Beyond activity and selectivity of the supported nanocomposite structures, the long-term stability of these materials in high-temperature reactive atmospheres is a key issue. As discussed in the introduction, stability at reactive conditions is a major concern in particular for nanoscaled catalyst materials due to their inherent thermodynamic instability. It is hence important to ascertain that the exceptional high-temperature stability of the Pt-BHA nanocomposite powders is not compromised in the attempt to design a hierarchical catalyst structure through supporting these powders on monolithic structures.

Because of the strong improvements in activity and selectivity seen for the Pt-BHA coated silica felt over the Pt-salt drop coated silica felt, we focused on the stability of this relatively novel type of supported catalyst. Continuous, extended (>20 h) CPOM reactive testing of silica felt with Pt-BHA was performed at a molar ratio CH_4:O_2 = 2.0 (N_2:O_2 = 4:1) and total flow rate of 4.0 SLM. Additionally, the effect of weight loading on catalyst stability was investigated by testing silica felts with "low" (0.0305 g), "medium" (0.0523 g), and "high" (0.0800 g) loadings of Pt-BHA. Fig. 9 shows the results of the catalyst stability testing for the low (left graph),

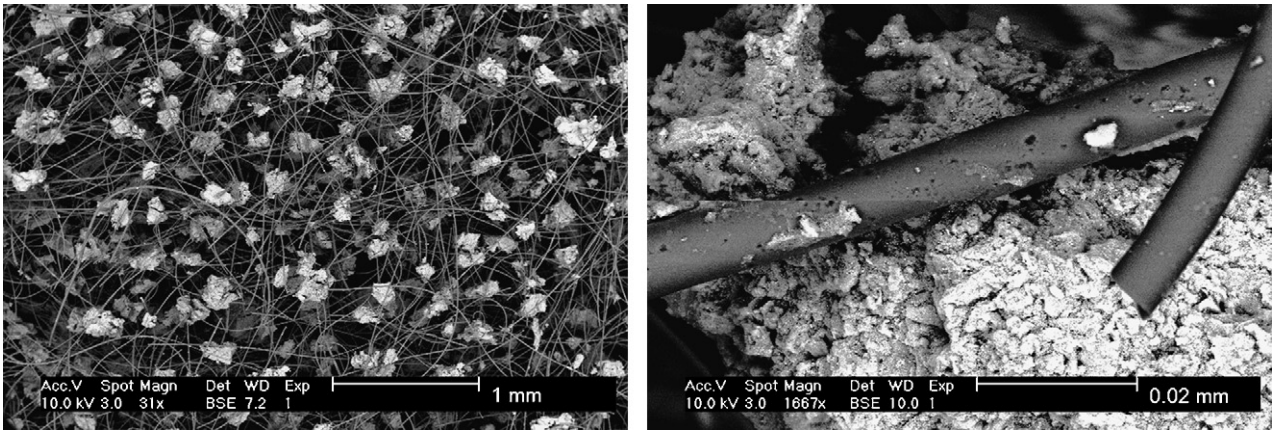

Fig. 10. SEM photos of silica felt strands after extended operation (>20 h) in partial oxidation of methane. CH_4:O_2 = 2.0, N_2:O_2 = 4:1, total flow rate = 4.0 SLM, autothermal operation.

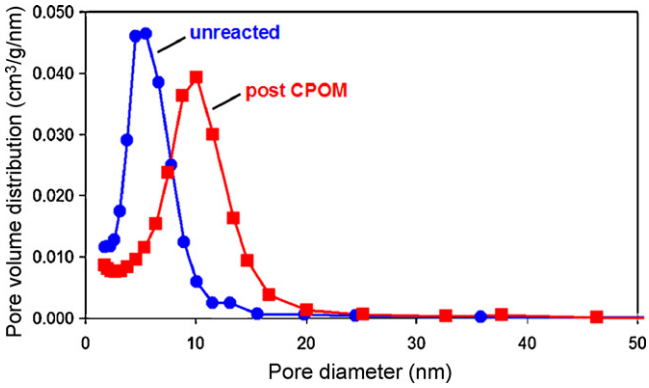

Fig. 11. Nitrogen porosimetry of Pt-BHA drop coated on silica felts (circles: as prepared and squares: after ~20 h of CPOM reaction at ~800 °C). Top: Nitrogen isotherm indicating a typical mesoporous material (adsorption, closed symbols; desorption, open symbols). Bottom: BJH analysis of desorption curve showing the pore size distribution.

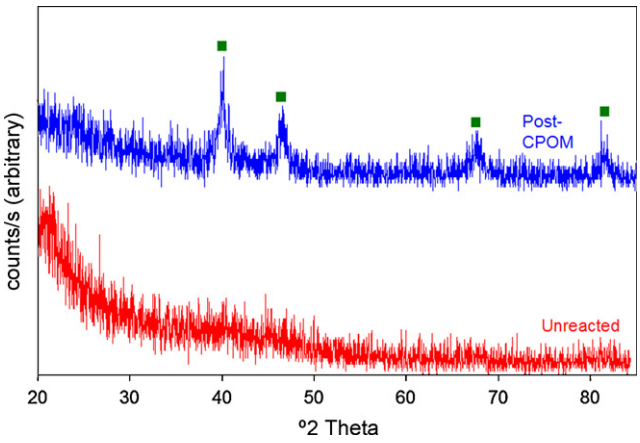

Fig. 12. X-ray diffraction patterns for unreacted and post-CPOM reaction silica felts coated with Pt-BHA. Squares indicate the location of metallic platinum reflexes.

medium (center) and high weight-loading felts (right graph) as methane conversion (triangles) and hydrogen and CO selectivities (squares and diamonds, respectively) versus molar CH_4:O_2 ratio.

One observes for the low weight-loading sample (left-most graph) a strong deactivation over the course of the experiment (~21 h) as indicated by the decrease in methane conversion and hydrogen selectivity by about 10%. This trend is weakened in the medium weight-loading sample (~3% decrease in H_2 selectivity and ~2% decrease in CH_4 conversion over ~23 h, center graph), and remains unchanged upon further increase from the medium to the high weight loading (right-most graph). Carbon monoxide selectivity remains stable ~84% for each of the three catalysts. In agreement

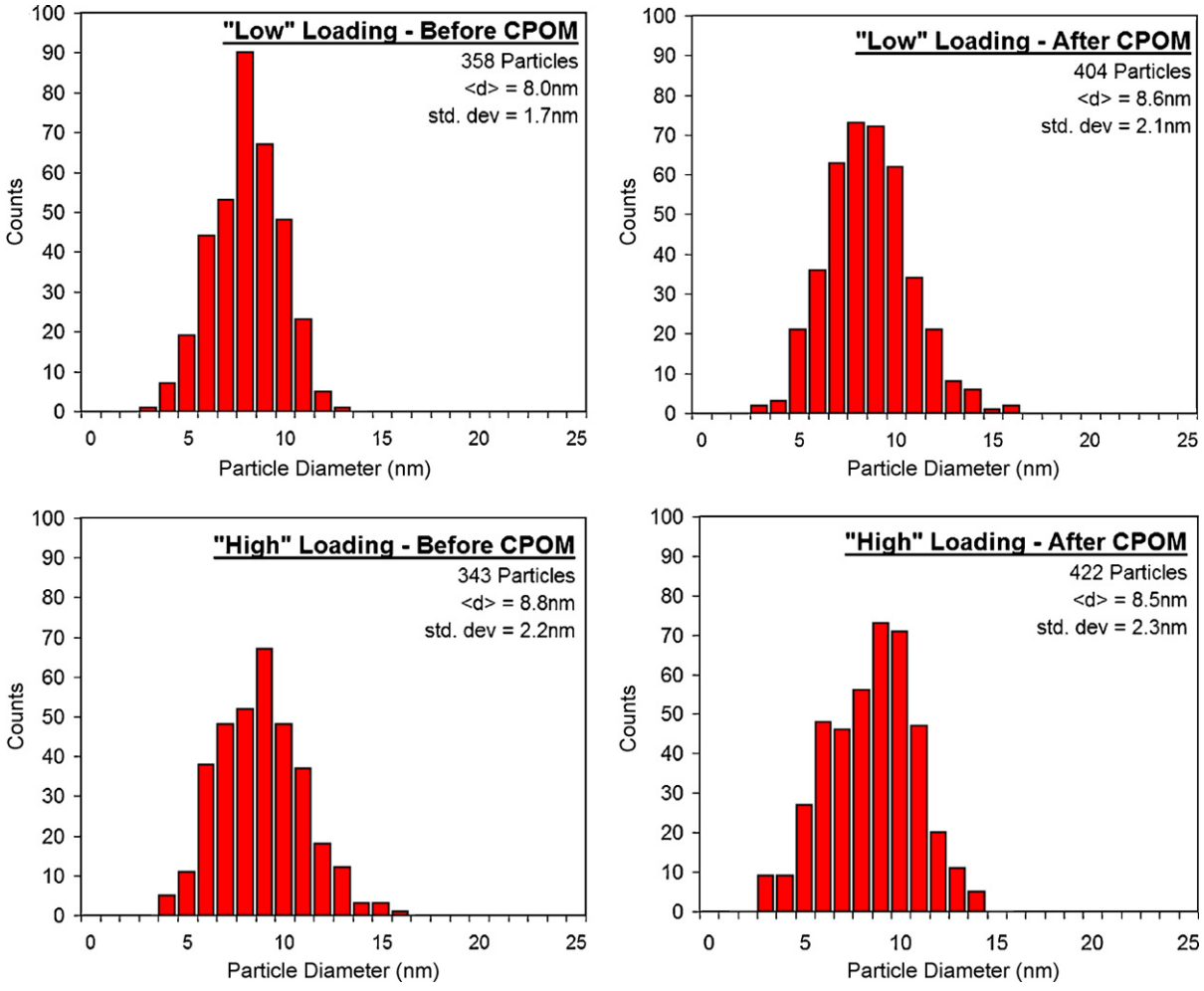

Fig. 13. Pt particle size distributions for "low" and "high" weight-loading Pt-BHA coated silica felts – both before and after ~20 h of CPOM testing – as determined from TEM images.

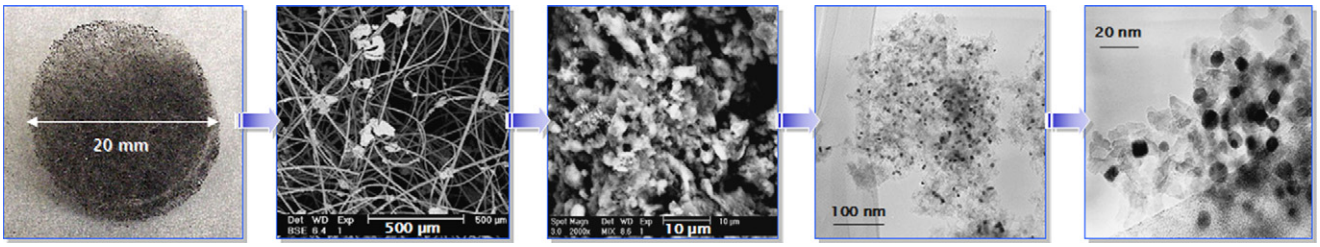

Fig. 14. TEM and SEM images and photo of the Pt-BHA coated silica felt catalyst, illustrating the hierarchical structuring of the catalyst across many length scales from the nanoscale (left) to the macroscale (right). From left to right: TEM images of Pt nanoparticles embedded in BHA; TEM image of Pt-BHA nanocomposite particulate; SEM image of the macropore structure of a nanocomposite particle; SEM image of Pt-BHA coated silica fibers; photo of the Pt-BHA coated silica felt catalyst.

with these observations, catalyst temperatures increased over the course of the 20 h, with a significant increase (from ~750 to ~840 °C) for the "low" weight loading, and a much more moderate increase (from ~730 to ~760 °C) for the "medium" and "high" samples.

In order to establish the reason for the deactivation experienced during the stability testing of silica felt supported Pt-BHA, a series of characterization studies (SEM, BJH, XRD, TEM) were performed to evaluate these composite materials before and after reactive testing.

SEM images of the various weight-loading catalysts after running the stability experiment ("high" weight loading pictured in Fig. 10) show that the texture and dispersion of the Pt-BHA material remains about the same as before reaction (compare to Fig. 6). The deactivation hence does not appear to be due to loss or sintering of the Pt-BHA agglomerates on the silica fibers.

Nitrogen porosimetry was used to further evaluate the pore structure of the Pt-BHA agglomerates attached to the silica felt for a fresh sample and a sample that had undergone long term CPOM reaction testing (~20 h on-stream). The adsorption and desorption isotherms for the fresh and post-CPOM samples are both typical type IV isotherms, indicating a mesoporous material with textural porosity. A Barrett–Joyner–Halenda (BJH) analysis of the desorption branch of the isotherm (Fig. 11) shows that the fresh sample (circles) has a smaller total pore volume than the post-reaction sample (squares; 0.377 cm^3/g vs. 0.392 cm^3/g), as well as a smaller average pore size (8.6 nm vs. 12.8 nm), and a larger specific surface area (106.2 m^2/g vs. 82.2 m^2/g, determined by BET analysis).

The results for the fresh sample are essentially unchanged from previous results for the pure Pt-BHA material [20] indicating that the structure of the Pt-BHA nanocomposite material is unaffected by the coating process. However, the results show a significant degree of restructuring of the material upon exposure to reaction conditions. This restructuring is due to changes in the BHA pore structure at temperatures in excess of ~800 °C, as also previously observed for a pure BHA material [33]. This restructuring leads to somewhat increased pore sizes and correspondingly decreased (total) surface area of the samples. Since the CPOM reaction exposes the catalyst to temperatures well in excess of 800 °C, it is not surprising to find a similar pore restructuring in the present samples. Overall, however, the results indicate that the catalyst structure remains intact.

X-ray diffraction (Fig. 12) of the fresh sample shows no discernible reflexes except for a broad feature at ~20°, indicative of amorphous silica from the silica felt itself. No reflexes representing BHA can be detected. This diffuse background does not change upon exposure to reaction conditions, in agreement with our previous finding that the BHA structure remains largely amorphous below ~1210 °C [20]. The Pt nanoparticles are too small to be picked up by XRD before reaction. After extended CPOM reaction, distinct Pt reflexes appear. A Debye–Scherrer fit of the dominant Pt reflex at ~40° 2θ yields a Pt particle size of 24.6 nm, well in excess of the expected particle size which is in the order of about 10 nm (see Fig. 3, right graph). However, this agrees with previous observations on these materials, where we found that while the majority of the Pt nanoparticles are well stabilized inside the porous BHA structure, a small fraction of Pt particles on the outer perimeter of the Pt-BHA agglomerates are not sufficiently held in place and hence sinter at higher temperatures. Since XRD is a volume sensitive technique, and since volume scales with the cube of the particle diameter, even a few sintered particles result in a strong apparent particle size increase.

To confirm this hypothesis, Pt particle size distributions in the silica felt supported Pt-BHA before and after extended exposure to CPOM were determined directly via TEM for both a low and a high weight-loading sample (Fig. 13). The results show that the Pt particle sizes remain indeed small and unchanged within experimental error ($d_P \sim 8$–9 nm with $\sigma \sim 2$ nm) for both catalyst samples. However, we also observe a very small, but significant, population of large Pt particles ($d_P > 100$ nm) in TEM (not shown) and a depletion of the outer perimeter of the Pt-BHA particulates of Pt nanoparticles after exposure to high temperatures (see also Fig. 2), confirming the above explanation of the large particle sizes determined via XRD.

These results point toward an explanation for why the medium and high weight-loading samples show a much less pronounced deactivation. These catalysts have sufficient platinum material remaining even after this "selective sintering" process to support the reaction and hence are able to sustain the reaction. Furthermore, this suggests that the deactivation process is limited to an initial decrease in activity – correlated with the (limited) agglomeration of unstable Pt nanoparticles – after which a stable, though slightly lower, level of activity should be reached. While we have previously demonstrated the long-term (>100 h) stability of the Pt-BHA powders [19], no attempt was made at a longer term stability test in the present study beyond the ~20 h studies presented here.

Overall, the results indicate that strong stabilizing effect of 'caging' the Pt nanoparticles inside the pore network of the nanocomposite that we observed before [20] is not compromised by the supporting process, and that the presented, simple form of supporting the nanocomposite powder results in a highly active, stable, and easy-to-handle catalyst.

4. Summary and conclusions

The design of hierarchically structured materials which incorporate nanoparticles in an easily accessible and high-temperature stable way is a major challenge on the way towards application of nanomaterials at industrial conditions. We presented a study on the supporting of a high-temperature stable nanocomposite platinum barium-hexaaluminate (Pt-BHA) powder onto a range of different, conventional and novel support materials (silica and alumina felts and foams, and extruded cordierite monoliths).

Silica felts showed the most uniform coatings, with coatings on alumina and silica foams being less uniform, and the extruded cordierite monoliths and alumina felts failing even basic mechanical tests after coating. These supported nanocomposite catalysts were tested in the catalytic partial oxidation of methane to synthesis gas (CPOM). The alumina foam and silica felt showed essentially unchanged activity and selectivity from the unsupported powder, while the extruded monolith and silica foam supported catalysts performed significantly worse. In comparison to their conventionally prepared counterparts (drop-coated from H_2PtCl_6), both the Pt-BHA coated alumina foam and silica felt showed improved methane conversion and hydrogen selectivity with over an order of magnitude less Pt loading.

Beyond its high activity and selectivity in CPOM, the Pt-BHA/silica-felt structured catalyst also constitutes a very flexible catalyst configuration which is easy to shape for specific geometrical requirements and safe to handle in industrial application. Typical problems associated with packed beds consisting of fine powders, such as high pressure drop and by-pass issues, can be completely eliminated. This catalyst configuration experienced only modest deactivation (especially at higher weight loading) over ~25 h of catalytic testing. The deactivation mechanism is associated with a loss of catalytic surface area due to sintering of a small population of un-stabilized Pt nanoparticles around the perimeter of the Pt-BHA particulates. However, the vast majority of Pt nanoparticles maintain their "nanosize" ($d \sim 8$–9 nm) during the high-temperature reaction, confirming the strong stabilizing effect of the BHA matrix reported before [19,20]. As little as ~50 mg of Pt-BHA on a single 2 mm long silica felt were sufficient to attain maximum hydrogen yields (~0.85). This corresponds to a reduction in the noble metal requirement by more than an order of magnitude in comparison to conventional metal-coated monoliths used previously.

Overall, we regard the presented work as a step towards bridging the gap between nanoscale science and ("macroscopic") technical application via hierarchical structuring of catalysts from the nanoscale to the macroscale as summarized in Fig. 14. In particular, such supported nanocomposite catalysts hold great potential for use in demanding environments, such as high-temperature, high-throughput conditions in fuel processing and similar energy-related applications.

Acknowledgements

Financial support by the Department of Energy—Hydrogen Fuel Initiative through grant #DE FG02 05ER46233 is gratefully acknowledged. The authors thank the University of Pittsburgh Department of Mechanical Engineering and Materials Science for access to the electron microscopy instrumentation.

References

[1] M. Haruta, Catal. Today 36 (1997) 153–166.
[2] K. Dick, T. Dhanasekaran, Z. Zhang, D. Meisel, J. Am. Chem. Soc. 124 (2002) 2312–2317.
[3] S. Costacurta, L. Biasetto, E. Pippel, J. Woltersdorf, P. Colombo, J. Am. Ceram. Soc. 90 (2007) 2172–2177.
[4] C. Danumah, S. Vaudreuil, L. Bonneviot, M. Bousmina, S. Giasson, S. Kaliaguine, Microporous Mesoporous Mater. 44–45 (2001) 241–247.
[5] D. Kuang, T. Brezesinski, B. Smarsly, J. Am. Chem. Soc. 126 (2004) 10534–10535.
[6] T. Sen, G.J.T. Tiddy, J.L. Casci, M.W. Anderson, Angew. Chem. Int. Ed. 42 (2003) 4649–4653.
[7] R.M. Heck, S. Gulati, R.J. Farrauto, Chem. Eng. J. 82 (2001) 149–156.
[8] F.C. Patcas, G.I. Garrido, B. Kraushaar-Czarnetzki, Chem. Eng. Sci. 62 (2007) 3984–3990.
[9] L. Kiwi-Minsker, I. Yuranov, B. Siebenhaar, A. Renken, Catal. Today 54 (1999) 39–46.
[10] I. Yuranov, L. Kiwi-Minsker, M. Slin'Ko, E. Kurkina, E.D. Tolstunova, A. Renken, Chem. Eng. Sci. 55 (2000) 2827–2833.
[11] V. Hoeller, D. Wegricht, I. Yuranov, L. Kiwi-Minsker, A. Renken, Chem. Eng. Technol. 23 (2000) 251–255.
[12] L. Kiwi-Minsker, I. Yuranov, E. Slavinskaia, V. Zaikovskii, A. Renken, Catal. Today 59 (2000) 61–68.
[13] V. Hoeller, D. Wegricht, L. Kiwi-Minsker, A. Renken, Catal. Today 60 (2000) 51–56.
[14] L. Kiwi-Minsker, I. Yuranov, V. Hoeller, A. Renken, Chem. Eng. Sci. 54 (1999) 4785–4790.
[15] B. Louis, C. Tezel, L. Kiwi-Minsker, A. Renken, Catal. Today 69 (2001) 365–370.
[16] H. Arai, M. Machida, Appl. Catal. A: Gen. 138 (1996) 161–176.
[17] A.J. Zarur, J.Y. Ying, Nature 403 (2000) 65–67.
[18] A. Mitri, D. Neumann, T. Liu, G. Veser, Chem. Eng. Sci. 59 (2004) 5527–5534.
[19] J. Schicks, D. Neumann, U. Specht, G. Veser, Catal. Today 81 (2003) 287–296.
[20] M. Kirchhoff, U. Specht, G. Veser, Nanotechnology 16 (2005) S401–S408.
[21] D.A. Hickman, L.D. Schmidt, Science 259 (1993) 343–346.
[22] D. Neumann, M. Kirchhoff, G. Veser, Catal. Today 98 (2004) 565–574.
[23] G. Veser, J. Frauhammer, U. Friedle, Catal. Today 61 (2000) 55–64.
[24] T. Liu, C. Snyder, G. Veser, Ind. Eng. Chem. Res., in press.
[25] D. Neumann, G. Veser, AIChE J. 51 (2005) 210–223.
[26] http://rsb.info.nih.gov/ij/, last accessed on 11/02/07.
[27] U. Friedle, G. Veser, Chem. Eng. Sci. 54 (1999) 1325–1332.
[28] P.D.F. Vernon, M.L.H. Green, A.K. Cheetham, A.T. Ashcroft, Catal. Lett. 6 (1990) 181–186.
[29] M. Huff, P.M. Torniainen, L.D. Schmidt, Catal. Today 21 (1994) 113–128.
[30] R. Horn, K.A. Williams, N.J. Degenstein, A. Bitsch-Larsen, D. Dalle Nogare, S.A. Tupy, L.D. Schmidt, J. Catal. 249 (2007) 380–393.
[31] E.P.J. Mallens, J.H.B.J. Hoebink, G.B. Marin, Catal. Lett. 33 (1995) 291–304.
[32] E.P.J. Mallens, J.H.B.J. Hoebink, G.B. Marin, J. Catal. 167 (1997) 43–56.
[33] T. Sanders, G. Veser, in preparation.